CHAPTER 3

Functionalized cyclophellitols are improved glucocerebrosidase inhibitors for generating neuropathic Gaucher model in zebrafish

Manuscript published as:

Artola M, **Kuo CL**, Lelieveld LT, Rowland RJ, van der Marel GA, Codée JDC, Boot RG, Davies DJ, Aerts JMFG, Overkleeft HS (2019) Functionalized Cyclophellitols Are Selective Glucocerebrosidase Inhibitors and Induce a Bona Fide Neuropathic Gaucher Model in Zebrafish. *J Am Chem Soc* **141**, 4214–4218.

ABSTRACT

Gaucher disease is caused by inherited deficiency in glucocerebrosidase (GBA, a retaining β-glucosidase), and deficiency in GBA constitutes the largest known genetic risk factor for Parkinson disease. In the past, animal models of Gaucher disease have been generated by treatment with the mechanism-based GBA inhibitors, conduritol B epoxide (CBE) and cyclophellitol. Both compounds however also target other retaining glycosidases, rendering generation and interpretation of such chemical knockout models complicated. Here it is demonstrated that cyclophellitol derivatives carrying a bulky hydrophobic substituent at C8 (cyclophellitol numbering) are potent and selective GBA inhibitors and that an unambiguous Gaucher animal model can be readily generated by treatment of zebrafish with these.

3.1 Introduction

Glucocerebrosidase (acid glucosylceramidase, GBA, E.C. 3.2.1.45,) is a lysosomal retaining β-glucosidase that belongs to the glycoside hydrolase (GH) 30 (www.cazy.org)[1] family and degrades the glycosphingolipid, glucosylceramide through a two-step Koshland double displacement mechanism (**Fig. 3.1A**). Inherited deficiency in GBA causes the most common autosomal recessive lysosomal storage disorder, Gaucher disease.[2] Individuals carrying heterozygous mutations in the gene coding for GBA do not develop Gaucher disease but have a remarkable increased risk for developing Parkinson disease (PD) and Lewy-body dementia.[3–5] Appropriate animal models linking impaired GBA functioning to Gaucher disease and Parkinson's disease are imperative both for understanding the pathophysiology of these diseases and for the development of effective treatments for these. Because complete genetic abrogation of GBA hampers animal viability due to skin permeability problems,[6] research models have been generated in the past in a chemical knockdown strategy by making use of the mechanism-based, covalent and irreversible retaining β-glucosidase inhibitor, conduritol B epoxide (CBE, **1**, **Fig. 3.1B**) or its close structural analogue, cyclophellitol (**2**, **Fig. 3.1B**).[7, 8] One complication in the use of these compounds is their relative lack of selectivity.[9] It has been found that cyclophellitol **2** is unsuited for creating a reliable Gaucher animal model because it targets GBA and GBA2 with about equal efficiency.[9] On the other hand, CBE **1** exhibits some GBA selectivity but it also inhibits lysosomal α-glucosidase (GAA),[10–13] non-lysosomal glucosylceramidase (GBA2),[14, 15] and lysosomal β-glucuronidase (GUSB)[16]. Effective mouse models can be generated with CBE **1**, but the therapeutic window is rather narrow and varies in cellular and animal models.

Recent research from the Aerts and Overkleeft group has revealed that functionalized cyclophellitol derivatives carrying a BODIPY substituent at C8 (cyclophellitol numbering, the primary carbon corresponding to C6 in glucose) are very potent and very selective activity-based probes (ABPs) for monitoring GBA activity *in vitro, in situ,* and *in vivo*.[17,18] The presence of a bulky and hydrophobic substituent at this position at once proved beneficial for GBA inactivation (ABPs **3** and **4**, (**Fig. 3.1C, D**)) proved to inhibit GBA in the nanomolar range, whereas cyclophellitol **2** is a high nanomolar to micromolar GBA inactivator and detrimental to inhibition of other retaining β-glucosidases. Following these studies, Vocadlo and co-workers designed a set of fluorogenic substrates featuring a fluorophore at C6 of a β-glucoside, the

aglycon of which carried a fluorescence quencher, compounds that proved to be very selective GBA substrates *in situ*.[19] These results altogether evoked the question whether cyclophellitols bearing a simple, hydrophobic moiety at C8, such as compounds **6** and **7** (**Fig. 3.1D**), would be suitable compounds for generating chemical knockdown Gaucher animal models. The validity of this reasoning is shown in the generation of a GBA-deficient *Dario rerio* zebrafish model, as revealed by the accumulation of elevated levels of the Gaucher harbinger lysolipid, glucosylsphingosine, using cyclophellitol derivatives **6** and **7**.

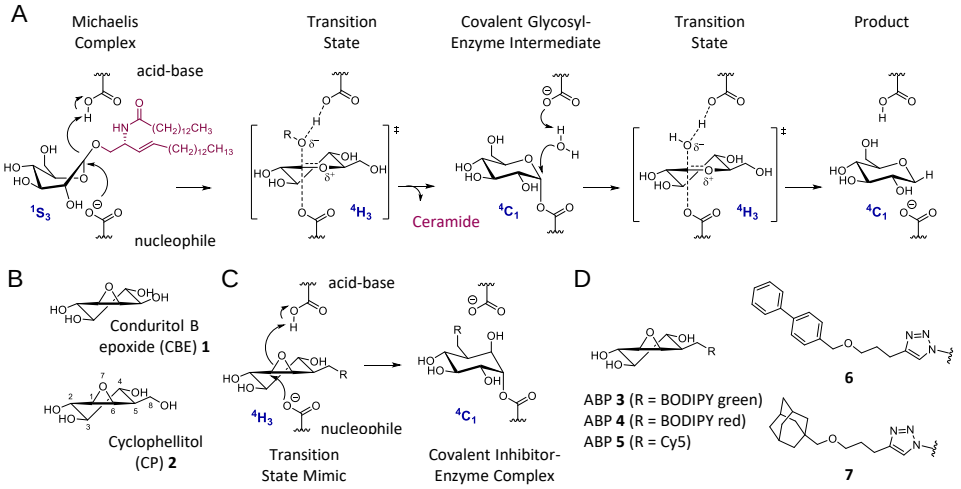

Figure 3.1. Structures and reaction mechanism of compounds in this chapter. A) Glucocerebrosidase (GBA) hydrolyses glucosylceramide in a two-step double displacement mechanism to yield glucose and ceramide. B) Chemical structure of CBE **1** and cyclophellitol **2**. C) Mechanism-based inactivation of GBA by glucopyranoside-configured cyclitol epoxides (shown for cyclophellitol). D) Structures of C6-extended cyclophellitol derivatives used in the here-presented studies: GBA1 activity-based probes ABPs **3**-**5** and selective inhibitors **6** and **7** (see for the full chemical structures of ABPs **3**-**5** and **8**-**14** in **Fig. 3.S1**).

3.2 Results and Discussion

3.2.1 Structural support for inhibitor design

At the onset of the studies, structural support was sought for the design of compounds **6** and **7**. The Cy5-functionalized cyclophellitol **5** was synthesized (Department of Bio-organic Chemistry, Leiden University) and a crystal structure of human recombinant GBA soaked with this ABP was obtained (University of York). As expected (**Fig. 3.2A**), the active site nucleophile (in both molecules of the asymmetric unit) had reacted with the epoxide to yield the covalently bound cyclitol in $^4C_1$-conformation, with the Cy5 moiety, via its flexible linker, clearly bound in

one molecule of the asymmetric unit (the differences may reflect crystal packing constraints in a soaking experiment) accommodated by a hydrophobic pocket in GBA. Previous studies on the bacterial glycoside hydrolase, *Thermoanaerobacterium xylanolyticum* TxGH116 β-glucosidase, a close homologue of human GBA2 with a conserved active site, instead showed an "inwards" position of O6 (**Fig. 3.S2A**) and a narrower and less hydrophobic pocket) (**Fig. 3.S2B**), which may partially mitigate against the binding of O6-functionaised probes, thus allowing sufficient discrimination for GBA over GBA2.[20, 21]

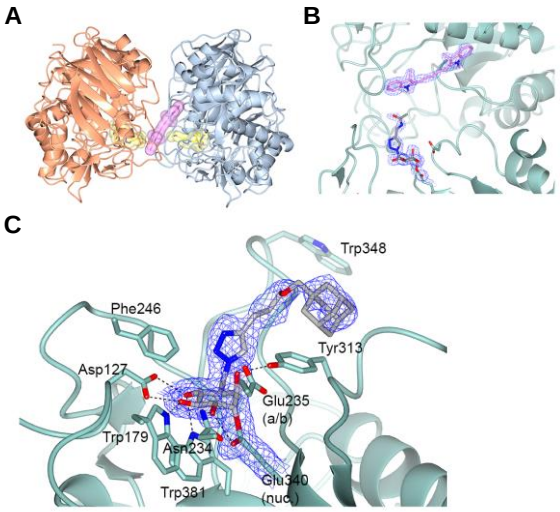

Figure 3.2. Structure of GBA reacted with ABP 5 and adamantyl-cyclophellitol 7. A) GBA dimer, with the cyclophellitol and linker moiety of **5** shaded in yellow, and a single observed Cy5 in pink. B) Zoomed view of a GBA monomer reacted with ABP **5**. C) Structure of GBA with adamantyl-cyclophellitol **7**. The linker-adamantyl moiety of **7** is observed in slightly different positions in the two molecules of the asymmetric unit (PDB Code 6Q6L, **Fig. 3.S2**) reflecting its binding through predominantly hydrophobic interactions.

Biphenyl-cyclophellitol **6** and adamantyl-cyclophellitol **7** were synthesized following adaptations of literature cyclophellitol syntheses (see **Appendix section 3.S2** for synthesis details) to generate superior selective GBA inhibitors for the generation of a Gaucher model zebrafish.[22, 23]

Although soaking of GBA crystals with **6** did not yield suitable structures for structural analysis (**Fig. 3.S2)**, soaking with **7** did (**Fig. 3.2C**), and again revealed binding of the

hydrophobic moiety (here, the adamantane) to the same hydrophobic cavity and pocket occupied by the O6 linker on Cy5 ABP **5**. Several hydrophobic residues, including Tyr313, Phe246, and Trp348 provide the wide cavity that is able to accommodate different hydrophobic O6 substituents which is absent in other human β-glucosidases and which provides the structural basis for the inhibitory (and substrate) preferences of GBA.

3.2.2 *In vitro* and *in vivo* activity of inhibitors

The *in vitro* activity and selectivity of compounds **6** and **7** towards GBA and the two major off-target glycosidases of CBE **1** (GBA2 and GAA)[9] were evaluated, by pre- incubating the inhibitors with recombinant human GBA (rGBA, Cerezyme), human GBA2 (from lysates of GBA2 overexpressed cells), and recombinant human GAA (rGAA, Myozyme) for 3 h, followed by enzymatic activity measurement. Both compound **6** and **7** were nanomolar inhibitors of rGBA (apparent IC_{50} values = 1.0 nM), which were 4,000-fold more potent than CBE **1** (apparent IC_{50} values = 4.28 μM) (**Fig. 3.3A**, **3.S3**) with improved lipophilic ligand efficiencies (LipE) (**Table 3.S2**). Both compounds **6** and **7** were rather inactive towards GBA2 and GAA (apparent IC_{50} values > 100 μM), similar to ABP **3** and **5** (**Fig. 3.3A**, **3.S4**). When comparing their selectivity towards GBA, both compounds **6** and **7** exhibited IC_{50} ratio **(**GBA2/GBA and GAA/GBA**)** of > 100,000, thus making them 4,000-times and 200-times more selective than CBE **1** (IC_{50} ratio **=** 23.6 for GBA2/GBA and 444 for GAA/GBA) (**Fig. 3.3A)**.

To evaluate the *in vivo* activity of compound **6** and **7**, compounds were added to the egg-water containing zebrafish (*Danio rerio*) embryos, and incubated for 5 days at 28 °C before subsequent homogenization and enzyme selectivity analysis by appropriate ABP labeling.[9, 24] Quantification of ABP-labeled bands revealed that compounds **6** and **7** had *in vivo* apparent IC_{50} values towards GBA of 4 to 6 nM, and that they were 5- to 70-fold more potent than ABP **3** or **5** and 7,500 fold more potent than CBE **1** (**Fig. 3.3B**, **3.S5**) in the zebrafish larvae. More importantly, an improved selective inactivation of GBA was achieved with both compounds **6** and **7**. At a concentration of 0.1-10 μM of compound **6** or **7**, ABP labeling of GBA with broad-spectrum retaining β-glucosidase ABP **8** (**Fig. 3.S1**) and GBA-specific ABP **5** was abrogated (**Fig. 3.3C**), while other enzymes such as GBA2 and LPH (**Figure 3.3C**), GAA, ER α-glucosidase GANAB, and lysosomal β-glucuronidase GUSB (**Fig. 3.S6A**, **3.S6B**) were not affected.

A

	CBE **1**	CP **2**	ABP **3**	ABP **5**	**6**	**7**
***In vitro* (nM)**						
rGBA	4.28 x 10^3 ± 500 [9]	29.6 ± 2.40 [9]	1.20 ± 0.30	3.20 ± 0.17	1.06 ± 0.19	0.96 ± 0.17
GBA2 (HEK2 93T lysate)	101 x 10^3 ± 20.1 x 10^3	29.7 ± 3.13	> 10^5	412 x 10^3 ± 10.1 x 10^3	> 10^5	> 10^5
rGAA	1.90 x 10^6 ± 192 x 10^3	> 10^5	> 10^5	> 10^5	> 10^5	> 10^5
Ratio (*In vitro*)						
GBA2/ GBA	24	1	> 10^5	> 10^4	> 10^5	> 10^5
GAA/ GBA	444	> 10^3	> 10^6	> 10^6	> 10^6	> 10^6

B

	CBE **1**	CP **2**	ABP **3**	ABP **5**	**6**	**7**
***In vivo* (*Danio Rerio* larvae) (nM)**						
GBA	4.41 x 10^4 [9]	83 [9]	31.6 ± 8.88	284 ± 31.5	5.85 ± 2.44	3.94 ± 1.21
GBA 2	8.90 x 10^5 [9]	59 [9]	> 10^4	> 10^4	> 10^4	> 10^4
GAA	9.55 x 10^6 [9]	> 10^5 [9]	> 10^4	> 10^4	> 10^4	> 10^4
Ratio (*in vivo*)						
GBA 2/ GBA	22.0	0.714	> 316	> 35.2	> 1,710	> 2,540
GAA / GBA	223	> 120	> 316	> 35.2	> 1,710	> 2,540

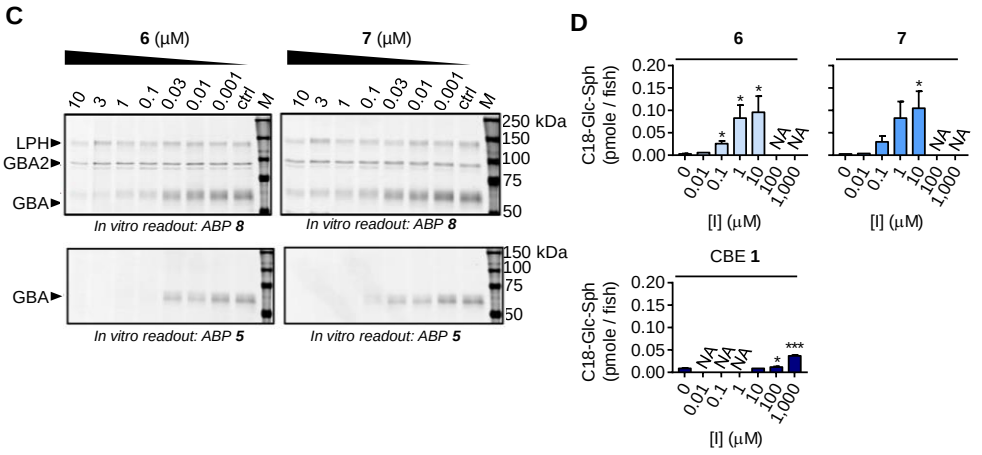

Figure 3.3. ***In vitro* and *in vivo* activity of compounds used in this study.** A) Apparent IC_{50} values for *in vitro* inhibition of GBA, GBA2 and GAA in recombinant enzymes (rGBA and rGAA) or overexpressed cell lysates (GBA2) by compounds **1**, **2**, **3**, **5**, **6** and **7**. Error ranges depict standard deviations from biological duplicates. B) Apparent IC_{50} values for *in vivo* inhibition in 5-day treated zebrafish embryo with compounds **1**, **2**, **3**, **5**, **6**, and **7**. Error ranges depict standard deviations from n = 12−24 individuals. C) Competitive ABPP in lysates of zebrafish treated in vivo with compounds **6** and **7** using broad-spectrum retaining β-glucosidase ABP **8** and selective GBA ABP **5** as readout. D) Glucosylsphingosine levels produced in zebrafish embryos treated for 5 days with inhibitors **6**, **7** or CBE **1**.[9] Error ranges depict standard deviations from n = 3 individuals. *N/A*, not analyzed; *, $p < 0.5$; ***, $p < 0.001$.

At 0.1-10 μM of inhibitor **6** or **7**, a 10- to 30-fold elevation in the level of glucosylsphingosine (GlcSph) was observed, which is known to be formed by acid ceramidase-mediated conversion of accumulating GlcCer in lysosomes.[25, 26] Therefore, this observation also strongly points to *in vivo* inactivation of lysosomal GBA. For comparison, reaching similar GlcSph levels in the zebrafish with CBE required 1,000 to 10,000-fold higher concentration in contrast with compounds **6** or **7** (**Fig. 3.3D**), concentrations at which GBA2 and GAA may also be targeted.

3.2.3 Brain permeability of inhibitors

Finally, the brain permeability of these new inhibitors was investigated, a crucial feature for their future application in the study of neuropathic Gaucher disease and Parkinson disease. Adult zebrafish of 3 months' age were treated with DMSO, ABP **3** or compound **7** (1,6 nmol/fish, approximately 4 μmol/kg) administered via food intake, and after 16 h brains and other organs were isolated, homogenized, and analyzed by ABP labeling using ABP **5** (GBA), ABP **8** (GBA2 + GBA), ABP **11** (GAA at pH 4.0 and ER α-glucosidase GANAB at pH 7.0), and ABP **13** (lysosomal β-glucuronidase GUSB) (**Fig. 3.S1**). Labeling of brain homogenate of adult zebrafish with ABP **5** resulted in considerable GBA labeling in control and ABP **3**-treated fish, but no labeling in brain homogenates from fish treated with compound **7** (**Fig. 3.4**). Labeling by the broad-spectrum β-glucosidase ABP **8** showed that GBA2 was not a target of compound **7**, nor was the lower running band (48 kDa), which is hypothesized to be the cytosolic β-glucosidase, GBA3 (E.C. 3.2.1.21).[27] It could be labeled (in lysates of zebrafish larvae) with the broad spectrum β-glucosidase ABP **8** at 0.1 μM[28] optimally at pH of 6.0 (**Fig. 3.S8**) and could be competed away by pre-incubating the lysates with another broad spectrum β-glucosidase ABP—ABP **10**, while not showing reactivity with the GBA-specific epoxide ABP **5** (**Fig. 3.S8**). It is noted that the expression level of this protein is likely variable among individual fish, as four out of six fish in the control group lacked this band (**Fig. 3.4**). In the visceral organs (both liver and spleen), both ABP **3** and compound **7** selectively abrogated GBA, while not affecting the labeling on other tested glycosidases (**Fig. 3.S7**).

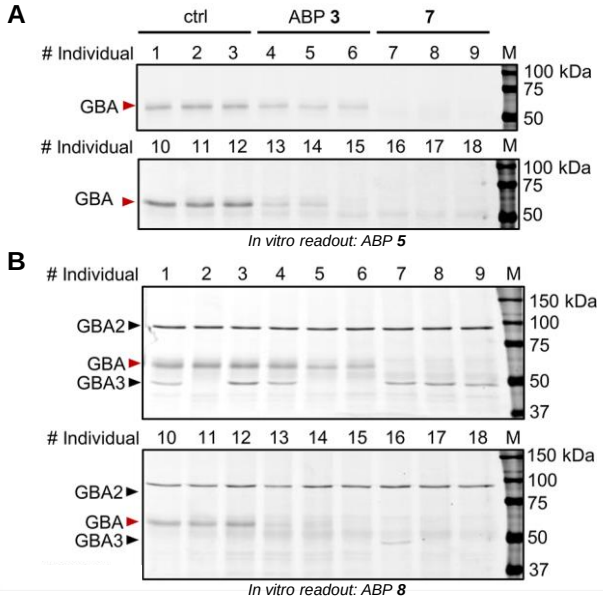

Figure 3.4. *In vivo* targets of ABP 3 and 7 in brains of adult zebrafish. Competitive ABPP in adult zebrafish homogenates with selective GBA ABP **5** or broad-spectrum retaining β-glucosidase ABP **8** as read-out.

3.3 Conclusion

To summarize, crystallographic studies aided the rational design of novel cyclophellitol analogues **6** and **7**, that turned out to be very potent and selective GBA inhibitors, also in zebrafish embryos and adult zebrafish (GBA2/GBA inhibition ratio > 1,000). Compound **7**, which also completely block GBA activity in the brain, should be superior to CBE **1** and CP **2** for generating GBA deficiency on demand in zebrafish, thus to create zebrafish models for neuropathic Gaucher disease, to assist research in the context of neuropathic GD and PD.

3.4 Experimental procedures

3.4.1 General materials and methods

Cyclophellitol (CP) **1** and the ABPs **3**, **4** and **8**–**14** were synthesized as described earlier[17, 27–30]. Conduritol B-epoxide (CBE) was purchased from Enzo Life Sciences (Farmingdale, NY, USA). Recombinant human GBA (rGBA, imiglucerase, Cerezyme®) and recombinant human GAA (rGAA, alglucosidase alfa, Myozyme) were obtained from Sanofi Genzyme (Cambridge, MA, USA). HEK293T (CRL-3216) cell lines were purchased from ATCC (Manassas, VA, USA). Cell lines were cultured in DMEM medium (Sigma-Aldrich, St. Lois, MO, USA), supplied with 10% (v/v) FCS, 0.1 % (w/v) penicillin/streptomycin, and 1 % (v/v) Glutamax, under 7 % CO_2 at 37°C. Zebrafish (*Danio rerio*) were handled and maintained as previously described.[9] Protein concentration was measured using Pierce BCA assay kit (Thermo Fisher Scientific, Waltham, MA, USA).

3.4.2 Preparation of cell lysates containing human GBA2

HEK293T cells overexpressing human GBA2 were generated as previously described[20]. For preparing lysates, cell pellets from two 15-cm culture dishes were resuspended in 1200 µL of lysis buffer (25 mM KH_2PO_4–K_2HPO_4, pH 6.5, protease inhibitor cocktail (EDTA-free, Roche, Basel, Switzerland), 2.5 U/mL benzonase) and incubated for 30 min on ice. The suspension was passed through a 30-gauge needle 10 times using a 1 mL syringe, and stored at –80°C.

3.4.3 *In vitro* activity of inhibitors on glycosidases measured by 4-MU substrates

In vitro apparent IC_{50} measurements with compounds (ABP **3**, ABP **5**, **6**, and **7**) in GBA (rGBA) followed the fluorogenic substrate methods described[9] previously at 3 h incubation time and 2 nM enzyme. For *in vitro* apparent IC_{50} measurements with compounds (CBE **1**, CP **2**, ABP **3**, ABP **5**, **6**, and **7**) in GBA2, 8 volumes of cell lysates (7 µg total protein/µL) containing overexpressed human GBA2 were firstly pre-incubated with 1 volume of ABP **4** (100 nM final concentration, 0.5% (v/v DMSO)) for 30 min at 37°C to selectively inhibit GBA activity. After which, lysates were incubated with 1 volume of compounds at various concentrations for 3 h at 37°C, before subsequent enzymatic assay for GBA2 activity described earlier.[9] For measurement in rGAA, 2.1 ng rGAA was prepared in 12.5 µL assay buffer (150 mM McIlvaine buffer, pH 4.0, 0.1% (w/v) bovine serum albumin (Sigma)), and incubated with compounds (CBE **1**, CP **2**, ABP

3, ABP **5**, **6**, and **7**) for 3 h at 37°C and subjected to GAA activity readout as described earlier ([enzyme] =19 nM during incubation).[9] All assays were performed in duplicate sets, each set with 3 technical replicates at each inhibitor concentration. DMSO concentration was kept at 1 % (v/v) in all assays during incubation with compounds. *In vitro* apparent IC_{50} values were calculated by fitting data with [inhibitor] vs response—various slope (four parameters) function using GraphPad Prism 7.0 software, and the average values and standard deviations were calculated from the two sets for each compound.

3.4.4 Zebrafish housing and breeding

Zebrafish were housed and maintained at the University of Leiden, the Netherlands, at a density of 40-50 adults per tank, on a cycle of 14 hours of light, 10 hours of darkness and at constant temperature of 28°C. The breeding of fish lines was approved by the local animal welfare committee (Instantie voor dierwelzijn, IvD) of the University of Leiden (license number: 10612). Experiments with embryos and larvae were performed before the free-feeding stage, not falling under animal experimentation law according the EU animal Protection Directive 2010/63/EU. Embryos and larvae were grown and incubated in egg water (60 µg/mL Instant Ocean Sera marin TM aquarium salts (Sera; Heinsberg, Germany) at constant temperature of 28 °C.

3.4.5 *In vivo* activity of inhibitors and fluorescent ABP labeling and detection in zebrafish larvae

For *in vivo* treatment of compounds (ABP **3**, ABP **5**, **6**, and **7**), a single fertilized embryo was seeded in each well of a 96-wells plate, and exposed to ABP **3** (0.001−10 µM), ABP **5** (0.0001−10 µM), **6** (0.001−10 µM) and **7** (0.001−10 µM) diluted in 200 µL egg water (0.5% (v/v) DMSO) for 120 hours at 28.5 °C. Per condition, n = 24 embryos were used. At 120 hours (5 dpf), larvae were collected, rinsed three times with egg water, fully aspirated, snap-frozen in liquid nitrogen and stored at –80 °C until homogenization in lysis buffer (without benzonase) at 4 µL/fish. Lysis was conducted by sonication with a Polytron PT 1300D sonicator (Kinematica, Luzern, Switzerland) on ice at 20% power for three seconds, and repeated three times. Samples containing 20–45 µg total protein were diluted in 14 µL lysis buffer, added with McIlvaine buffer at various pHs, and subjected to ABP detection at a final volume of 32 µL for 30 min at 37 °C using the following conditions: GBA with McIlvaine buffer pH 5.2 (with 0.1 % (v/v) Triton X-100 and 0.2 % (w/v) sodium taurocholate (Sigma)), and 200 nM ABP **4** or ABP **5**; β-glucosidases (GBA, GBA2, GBA3, LPH) with McIlvaine buffer pH 5.5 and 100 nM ABP **8** or ABP **9**; GAA

with McIlvaine buffer pH 4.0 and pre-incubation with 200 nM ABP **10**, before incubation with 500 nM ABP **11** or 3 μM ABP **12**; GANAB with McIlvaine buffer pH 7.0 and pre-incubation with 200 nM ABP **10**, before incubation with 500 nM ABP **11** or ABP **12**; GUSB with McIlvaine buffer pH 5.0 and pre-incubation with 200 nM ABP **10**, before incubation with 200 nM ABP **13** or ABP **14**. After ABP incubation, proteins were denatured and separated by SDS-PAGE, and analysed according to the previously described method.[9] Coomassie staining was used to assess total protein loading.

3.4.6 *In vivo* activity of inhibitors in adult zebrafish

Surplus wild-type adult zebrafish of 3 months of age were administrated with a single dose of food grain mixed with DMSO, ABP **3** or **7** (1.6 nmol/fish, approximately 4 μmol/kg, $n = 3$ for each treatment) in $n = 2$ sets, according to project license AVD1060020184725,1-04 held by Dr. R.G. Boot. An initial experiment was performed with 3 adult zebrafish and the effect was confirmed by additional 3 individuals per experimental condition. Zebrafish were sacrificed after 24 h using Tricaine (250 mg/L), organs were harvested, snap-frozen in liquid nitrogen and stored at -80°C until use. Food grain consisted of Gemma micro mixed with Gemma diamond (Skretting, Stavanger, Norway). Lysis was performed with 50 μL lysis buffer (without benzonase) per sample, and lysates containing 20–60 μg total protein were analyzed by ABP method for GBA, GBA2, GAA, GANAB, and GUSB, as described in the previous section.

3.4.7 Sphingolipid extraction and analysis by mass spectrometry in treated zebrafish larvae

Zebrafish embryos at 8 hours post fertilization were seeded in 12-well plates (15 fish/well, 3 mL egg water/well) and treated with CBE **1** (10–1,000 μM)[9], **6** (0.001−10 μM) or **7** (0.001−10 μM) for 112 hours at 28 °C. Thereafter, zebrafish larvae were washed three times with egg water, and collected in clean screw-cap Eppendorf tubes (three tubes of three larvae per inhibitor concentration). Lipids were extracted and measured according to methods described previously.[31] Briefly, after removing of the egg water, 20 μL of ^{13}C-GlcSph[32] from concentration of 0.1 pmol μL^{-1} in MeOH, 480 μL MeOH, and 250 μL $CHCl_3$ were added to the sample, stirred, incubated for 30 min at RT, sonicated (5 x 1 min in sonication water bath), and centrifuged for 10 min at 15,700 g. Supernatant was collected in a clean tube, where 250 μL $CHCl_3$ and 450 μL 100 mM formate buffer (pH 3.2) were added. The sample was stirred and centrifuged, the upper phase was transferred to a clean tube. The lower phase was extracted with 500 μL MeOH and

450 μL formate buffer. The upper phases were pooled and taken to dryness in a vacuum concentrator at 45 °C. The residue was extracted with 700 μL butanol and 700 μL water, stirred and centrifuged. The upper phase (butanol phase) was dried and the residue was dissolved in 100 μL MeOH. 10 μL of this sample was injected to the LC-MS for lipid measurement. Two-tailed unpaired t-test was performed in Prism 7.0 software (GraphPad) to derive statistical significance, where $p < 0.05$ was considered significant.

3.5 References

1 Lombard V, Golaconda Ramulu H, Drula E, Coutinho PM, & Henrissat B (2014) The Carbohydrate-Active Enzymes Database (CAZy) in 2013. *Nucleic Acids Res* **42**, 490–495.

2 Brady RO, Kanfer JN, Bradley RM & Shapiro D (1966) Demonstration of a Deficiency of Glucocerebroside-Cleaving Enzyme in Gaucher's Disease. *J Clin Invest* **45**, 1112–1115.

3 Schapira AHV (2015) Glucocerebrosidase and Parkinson Disease: Recent Advances. *Mol Cell Neurosci* **66**, 37–42.

4 Tsuang D, Leverenz JB, Lopez OL, Hamilton RL, Bennett DA, Schneider JA, Buchman AS, Larson EB, Crane PK, Kaye JA Kramer P, Woltjer R, Kukull W, Nelson PT, Jicha GA, Neltner JH, Galasko D, Masliah E, Trojanowski JQ, Schellenberg GD, Yearout D, Huston H, Fritts-Penniman A, Mata IF, Wan JY, Edwards KL, Montine TJ & Zabetian CP (2012) GBA Mutations Increase Risk for Lewy Body Disease with and without Alzheimer Disease Pathology. *Neurology* **79**, 1944–1950.

5 Sidransky E, Nalls MA, Aasly JO, Aharon-Peretz J, Annesi G, Barbosa ER, Bar-Shira A, Berg D, Bras J, Brice A, Chen CM, Clark LN, Condroyer C, De Marco EV, Dürr A, Eblan MJ, Fahn S, Farrer MJ, Fung HC, Gan-Or Z, Gasser T, Gershoni-Baruch R, Giladi N, Griffith A, Gurevich T, Januario C, Kropp P, Lang AE, Lee-Chen GJ, Lesage S, Marder K, Mata IF, Mirelman A, Mitsui J, Mizuta I, Nicoletti G, Oliveira C, Ottman R, Orr-Urtreger A, Pereira LV, Quattrone A, Rogaeva E, Rolfs A, Rosenbaum H, Rozenberg R, Samii A, Samaddar T, Schulte C, Sharma M, Singleton A, Spitz M, Tan EK, Tayebi N, Toda T, Troiano AR, Tsuji S, Wittstock M, Wolfsberg TG, Wu YR, Zabetian CP, Zhao Y & Ziegler SG (2009) Multicenter Analysis of Glucocerebrosidase Mutations in Parkinson's Disease. *N Engl J Med* **361**, 1651–1661.

6 Holleran WM, Ginns EI, Menon GK, Grundmann JU, Fartasch M, McKinney CE, Elias PM & Sidransky E (1994) Consequences of β-Glucocerebrosidase Deficiency in Epidermis. Ultrastructure and Permeability Barrier Alterations in Gaucher Disease. *J Clin Invest* **93**, 1756–1764.

7 Farfel-Becker T, Vitner EB & Futerman AH (2011) Animal Models for Gaucher Disease Research. *Dis Model Mech* **4**, 746–52.

8 Vardi A, Zigdon H, Meshcheriakova A, Klein AD, Yaacobi C, Eilam R, Kenwood BM, Rahim AA, Massaro G, Merrill AH Jr, Vitner EB & Futerman AH (2016) Delineating Pathological Pathways in a Chemically Induced Mouse Model of Gaucher Disease. *J Pathol* **239**, 496–509.

9 Kuo CL, Kallemeijn WW, Lelieveld LT, Mirzaian M, Zoutendijk I, Vardi A, Futerman AH, Meijer AH, Spaink HP, Overkleeft HS, Aerts JMFG, Artola M (2019) In Vivo Inactivation of Glycosidases by Conduritol B Epoxide and Cyclophellitol as Revealed by Activity-Based Protein Profiling. *FEBS J* **286**, 584– 600.

10 Quaroni A, Gershon E & Semenza G (1974) Affinity Labeling of the Active Sites in the Sucrase-Isomaltase Complex from Small Intestine. *J Biol Chem* **249**, 6424–6433.

11 Yang SJ, Ge SG, Zeng YC & Zhang SZ (1985) Inactivation of α-Glucosidase by the Active-Site-Directed Inhibitor, Conduritol B Epoxide. *BBA - Protein Struct Mol Enzymol* **828**, 236–240.

12 Hermans MM, Krooss MA, van Beeurnens J, Oostras BA, Reuser AJ (1991) Human Lysosomal alpha-Glucosidase. Characterization of the Catalytic Site. *Biochemistry* **266**, 13507–13512.

13 Braun H, Legler G, Deshusses J & Semenza G (1977) Stereospecific Ring Opening of Conduritol-B-Epoxide by an Active Site Aspartate Residue of Sucrase-Isomaltase. *BBA - Enzymol* **483**, 135–140.

14 van Weely S, Brandsma M, Strijland A, Tager JM & Aerts JMFG (1993) Demonstration of the Existence of a Second, Non-Lysosomal Glucocerebrosidase That Is Not Deficient in Gaucher Disease. *BBA - Mol Basis Dis* **1181**, 55–62.

15 Ridley CM, Thur KE, Shanahan J, Thillaiappan NB, Shen A, Uhl K, Walden CM, Rahim AA, Waddington SN, Platt FM & van der Spoel AC (2013) β-Glucosidase 2 (GBA2) Activity and Imino Sugar Pharmacology. *J Biol Chem* **288**, 26052–26066.

16 Hara A & Radin NS (1979) Enzymic Effects of β-Glucosidase Destruction in Mice Changes in Glucuronidase Levels. *BBA - Gen Subj* ***582***, 423–433.

17 Witte MD, Kallemeijn WW, Aten J, Li KY, Strijland A, Donker-Koopman WE, van den Nieuwendijk AM, Bleijlevens B, Kramer G, Florea BI, Hooibrink B, Hollak CE, Ottenhoff R, Boot RG, van der Marel GA, Overkleeft HS & Aerts JM (2010) Ultrasensitive in Situ Visualization of Active Glucocerebrosidase Molecules. *Nat Chem Biol* **6**, 907–913.

18 Herrera Moro Chao D, Kallemeijn WW, Marques AR, Orre M, Ottenhoff R, van Roomen C, Foppen E, Renner

MC, Moeton M, van Eijk M, Boot RG, Kamphuis W, Hol EM, Aten J, Overkleeft HS, Kalsbeek A & Aerts JM (2015) Visualization of Active Glucocerebrosidase in Rodent Brain with High Spatial Resolution Following in Situ Labeling with Fluorescent Activity Based Probes. *PLoS One* **10**, e0138107.

19 Yadav AK, Shen DL, Shan X, He X, Kermode AR, Vocadlo DJ (2015) Fluorescence-Quenched Substrates for Live Cell Imaging of Human Glucocerebrosidase Activity. *J Am Chem Soc* **137**, 1181–1189.

20 Lahav D, Liu B, van den Berg RJBHN, van den Nieuwendijk AMCH, Wennekes T, Ghisaidoobe AT, Breen I, Ferraz MJ, Kuo CL, Wu L, Geurink PP, Ovaa H, van der Marel GA, van der Stelt M, Boot RG, Davies GJ, Aerts JMFG & Overkleeft HS (2017) A Fluorescence Polarization Activity-Based Protein Profiling Assay in the Discovery of Potent, Selective Inhibitors for Human Nonlysosomal Glucosylceramidase. *J Am Chem Soc* **139**, 14192–14197.

21 Charoenwattanasatien R, Pengthaisong S, Breen I, Mutoh R, Sansenya S, Hua Y, Tankrathok A, Wu L, Songsiriritthigul C, Tanaka H, Williams SJ, Davies GJ, Kurisu G & Cairns JR (2016) Bacterial β-Glucosidase Reveals the Structural and Functional Basis of Genetic Defects in Human Glucocerebrosidase 2 (GBA2). *ACS Chem Biol* ***11***, 1891–1900.

22 Berger J, Lecourt S, Vanneaux V, Rapatel C, Boisgard S, Caillaud C, Boiret-Dupré N, Chomienne C, Marolleau JP, Larghero J & Berger MG (2010) Glucocerebrosidase Deficiency Dramatically Impairs Human Bone Marrow Haematopoiesis in an in Vitro Model of Gaucher Disease. *Br J Haematol* **150**, 93–101.

23 Schueler UH, Kolter T, Kaneski CR, Zirzow GC, Sandhoff K & Brady RO (2004) Correlation between Enzyme Activity and Substrate Storage in a Cell Culture Model System for Gaucher Disease. *J Inherit Metab Dis* **27**, 649–658.

24 Kuo CL, van Meel E, Kytidou K, Kallemeijn WW, Witte M, Overkleeft HS, Artola ME & Aerts JM (2018) Activity-Based Probes for Glycosidases: Profiling and Other Applications. *Methods Enzymol* **598**, 217– 235.

25 Dekker N, van Dussen L, Hollak CE, Overkleeft H, Scheij S, Ghauharali K, van Breemen MJ, Ferraz MJ, Groener JE, Maas M, Wijburg FA, Speijer D, Tylki-Szymanska A, Mistry PK, Boot RG & Aerts JM (2011) Elevated Plasma Glucosylsphingosine in Gaucher Disease: Relation to Phenotype, Storage Cell Markers, and Therapeutic Response. *Blood* **118**, e118–e127.

26 Ferraz MJ, Marques AR, Appelman MD, Verhoek M, Strijland A, Mirzaian M, Scheij S, Ouairy CM, Lahav D, Wisse P, Overkleeft HS, Boot RG & Aerts JM (2016) Lysosomal Glycosphingolipid Catabolism by Acid Ceramidase: Formation of Glycosphingoid Bases during Deficiency of Glycosidases. *FEBS Lett* **590**, 716–725.

27 Schröder SP, van de Sande JW, Kallemeijn WW, Kuo CL, Artola M, van Rooden EJ, Jiang J, Beenakker TJM, Florea BI, Offen WA, Davies GJ, Minnaard AJ, Aerts JMFG, Codée JDC, van der Marel GA & Overkleeft HS (2017) Towards Broad Spectrum Activity-Based Glycosidase Probes: Synthesis and Evaluation of Deoxygenated Cyclophellitol Aziridines. *Chem Commun* **53**, 12528–12531.

28 Jiang J, Beenakker TJ, Kallemeijn WW, van der Marel GA, van den Elst H, Codée JD, Aerts JM & Overkleeft HS (2015) Comparing Cyclophellitol N-Alkyl and N-Acyl Cyclophellitol Aziridines as Activity-Based Glycosidase Probes. *Chemistry* **21**, 10861–10869.

29 Jiang J, Kuo CL, Wu L, Franke C, Kallemeijn WW, Florea BI, van Meel E, van der Marel GA, Codée JD, Boot RG, Davies GJ, Overkleeft HS & Aerts JM (2016) Detection of Active Mammalian GH31 α-Glucosidases in Health and Disease Using in-Class, Broad-Spectrum Activity-Based Probes. *ACS Cent Sci* **2**, 351–358.

30 Wu L, Jiang J, Jin Y, Kallemeijn WW, Kuo CL, Artola M, Dai W, van Elk C, van Eijk M, van der Marel GA, Codée JDC, Florea BI, Aerts JMFG, Overkleeft HS & Davies GJ. (2017) Activity-Based Probes for Functional Interrogation of Retaining β-Glucuronidases. *Nat Chem Biol* **13**, 867–873.

31 Mirzaian M, Wisse P, Ferraz MJ, Marques ARA, Gabriel TL, van Roomen CPAA, Ottenhoff R, van Eijk M, Codée JDC, van der Marel GA, Overkleeft HS & Aerts JM (2016) Accurate Quantification of Sphingosine-1-Phosphate in Normal and Fabry Disease Plasma, Cells and Tissues by LC-MS/MS with13C-Encoded Natural S1P as Internal Standard. *Clin Chim Acta* **459**, 36–44.

32 Wisse P, Gold H, Mirzaian M, Ferraz MJ, Lutteke G, Van Den Berg RJB H N, Van Den Elst H, Lugtenburg J, Van Der Marel GA, Aerts JMFG, Codée JDC & Overkleeft HS (2015) Synthesis of a Panel of Carbon-13-Labelled (Glyco)sphingolipids. *European J Org Chem* **2015**, 2661-2677.

APPENDIX

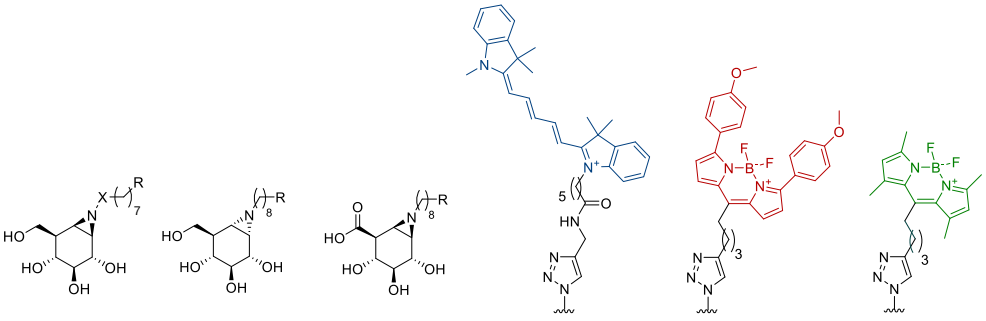

Figure 3.S1. Chemical structures of ABPs 8-14 used in this work. Code for each ABP: ABP **8** (JJB367), ABP **9** (JJB75), ABP **10** (JJB70), ABP **11** (JJB383), ABP **12** (JJB347), ABP **13** (JJB392), and ABP **14** (JJB391).

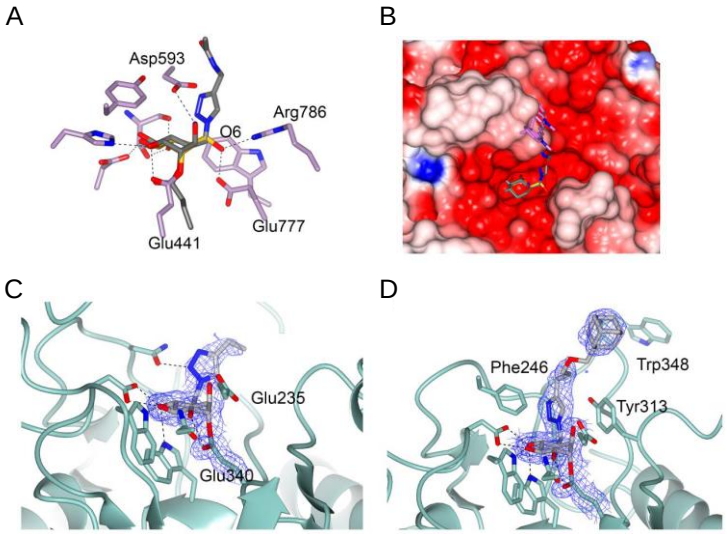

Figure 3.S2. Accommodation of O6-derivatized ligands in GBA1 and GBA2. A) Overlay of the bacterial GBA2 homology TxGH116 (PDB 5NCX, carbon-atoms colored lavender, aziridine complex bound to Glu441 in yellow) with the GBA1 complex with **5** reported here (grey carbons). Of note is the "inwards" orientation of O6, via interactions with Arg786 and Glu777 and the constricted space by virtue of the position of Asp593. B) Partial electrostatic surface of TxGH116 overlaid with the ligand coordinates for **5** bound to GBA1 (this work) overlaid (indicating potential steric clashes were the ligand bound exactly as in GBA1). Together these overlays suggest that TXGH116 is less able to accommodate O6 substituted ligands, at least to the extent that O6 substituted ligands gain sufficient discriminatory power for GBA1/GBA2. C) Structure of GBA reacted with biphenyl-cyclophellitol **6** and adamantyl-cyclophellitol. The biphenyl moiety is not visible and just the cyclophellitol-GBA complex structure is observed (PDB Code 6Q6N). D) The linker-adamantyl moiety of **6** is observed in slightly different positions in the two molecules of the asymmetric unit (PDB Code 6Q6L) reflecting its binding through predominantly hydrophobic interactions and the flexibility of its accommodation in crystal.

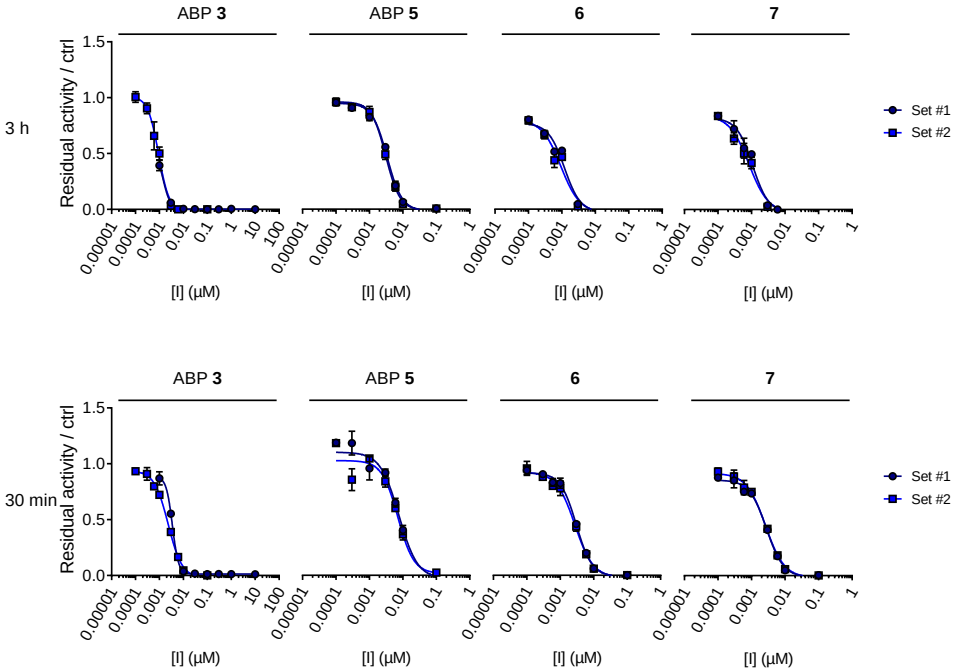

Figure 3.S3. *In vitro* inhibition curves of ABPs 3 and 5 and inhibitors 6 and 7 on rGBA: 3 h *vs* 30 min incubation.

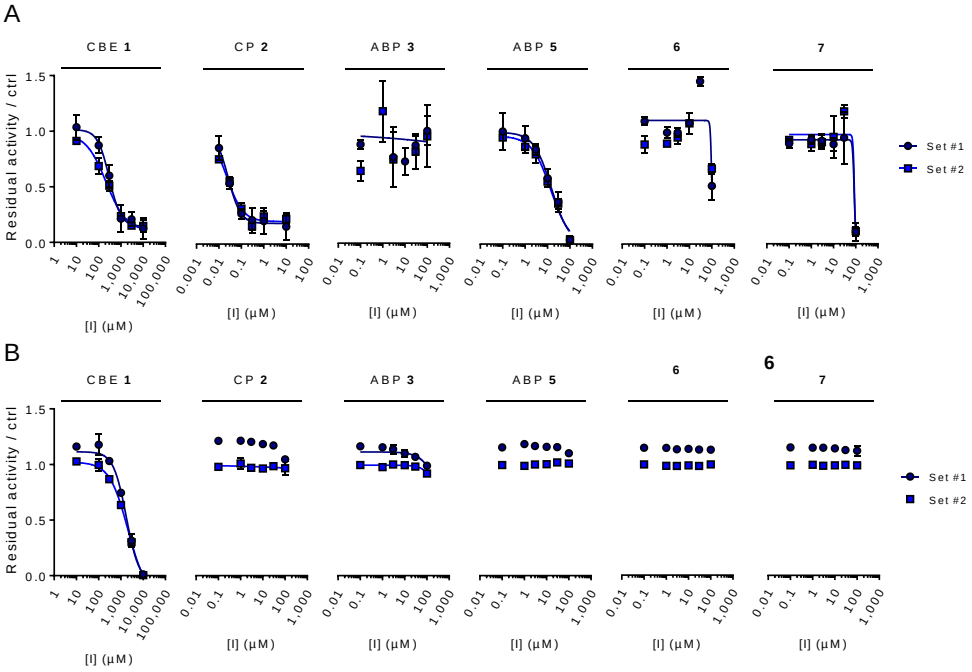

Figure 3.S4. *In vitro* inhibition curves of CBE 1, CP 2, ABPs 3 and 5, and inhibitors 6 and 7 on GBA2 from A) overexpressed cell lysates and on B) rGAA.

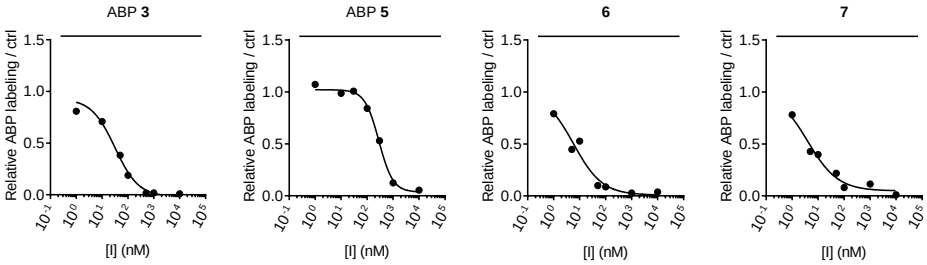

Figure 3.S5. Inhibition curves for i*n vivo* GBA inactivation in zebrafish larvae by ABPs 3 and 5, and inhibitors 6 and 7 quantified by ABP labeling.

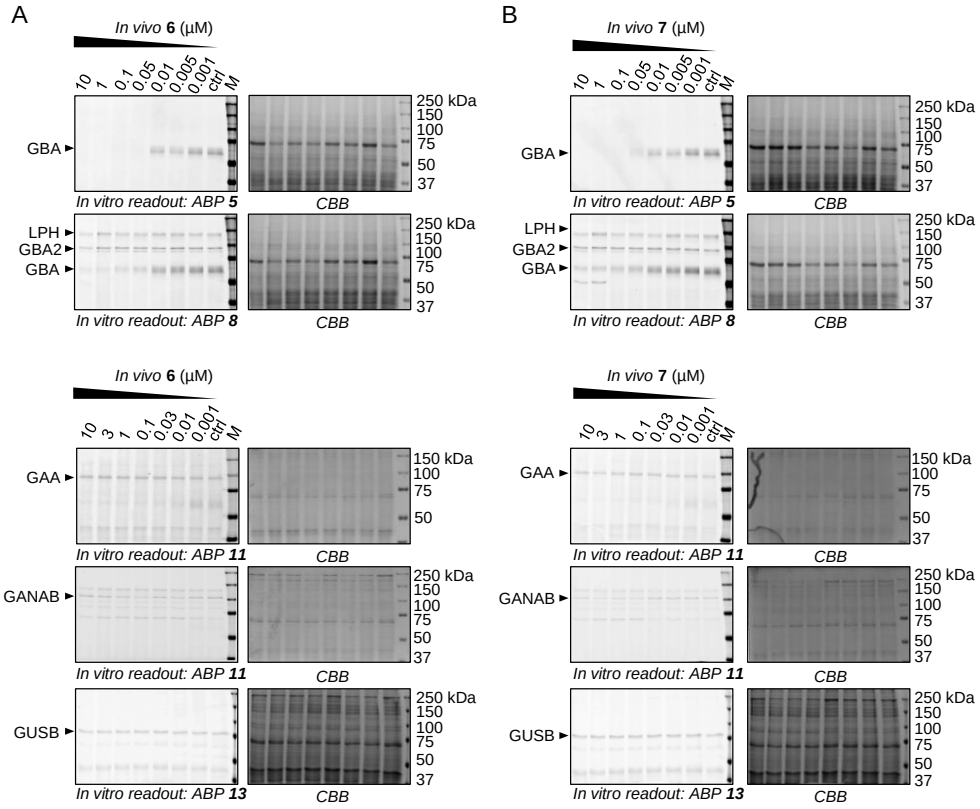

Figure 3.S6 (continued, 1 of 2).

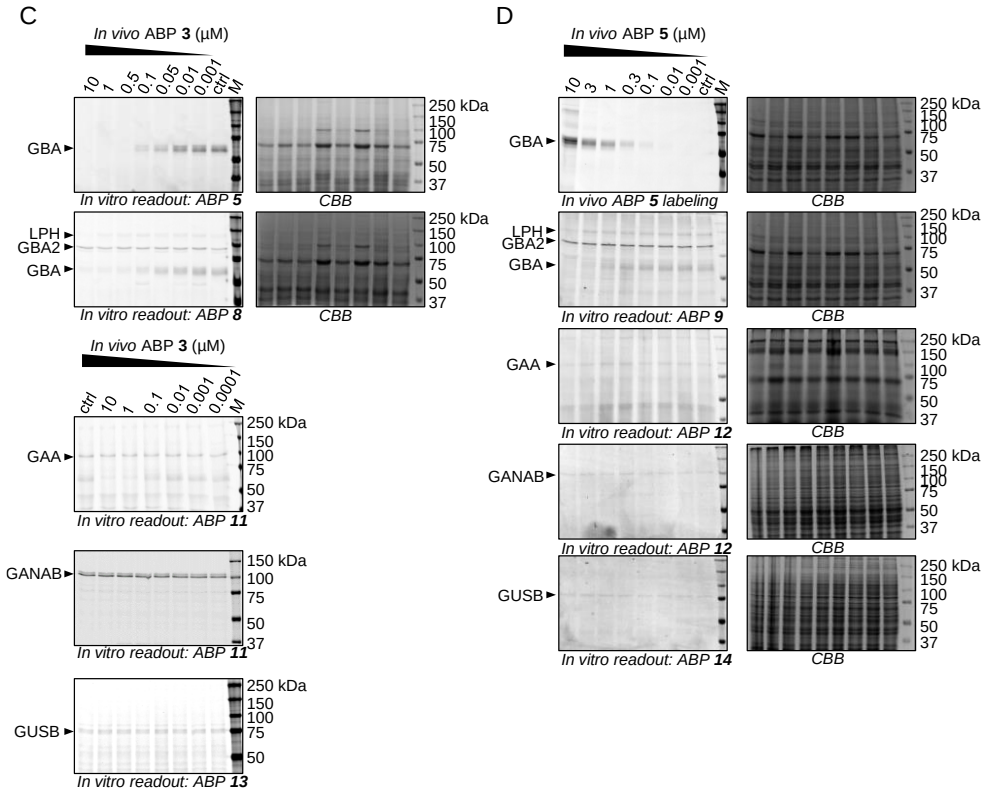

Figure 3.S6. ***In vivo*** **targets of A) inhibitor 6, B) inhibitor 7, C) ABP 3, and D) ABP 5 in zebrafish larvae revealed by competitive ABPP.** ***CBB*****, coomassie brilliant blue stain.**

A

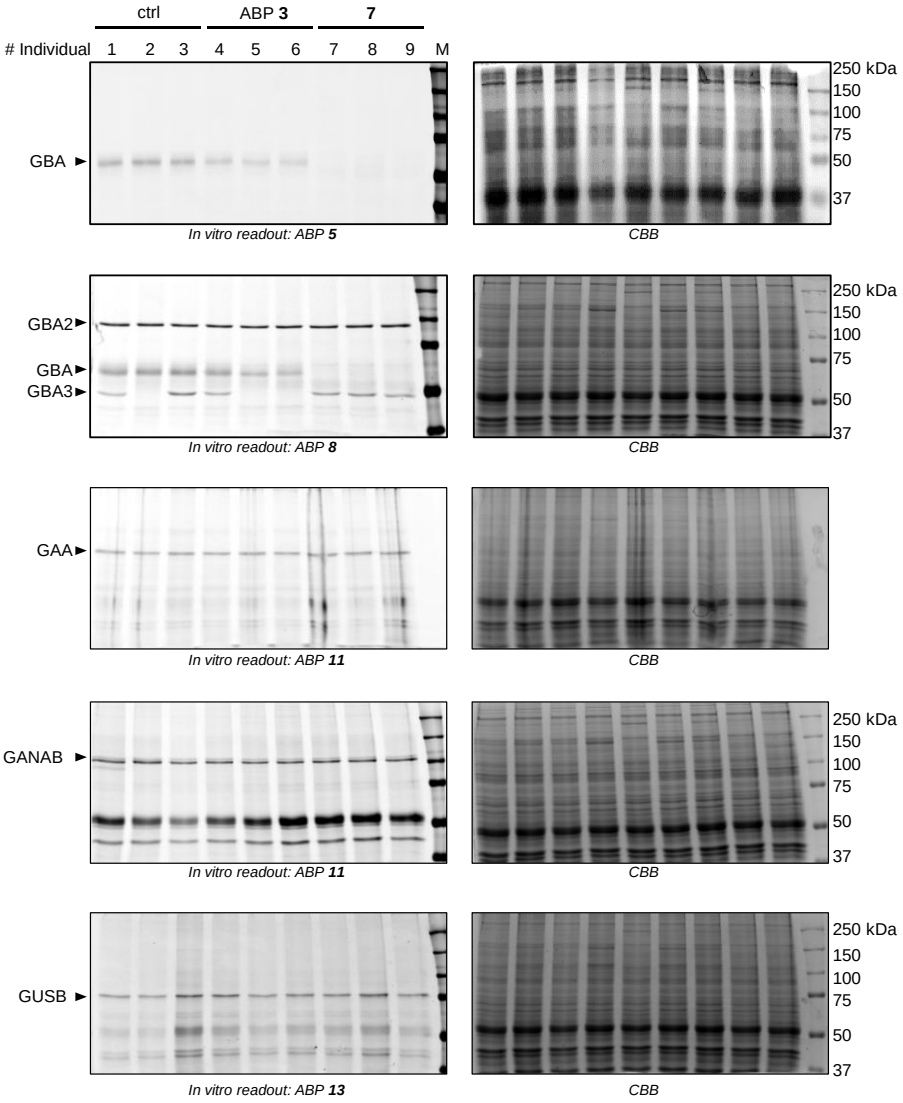

Figure 3.S7 (continued, 1 of 4).

B

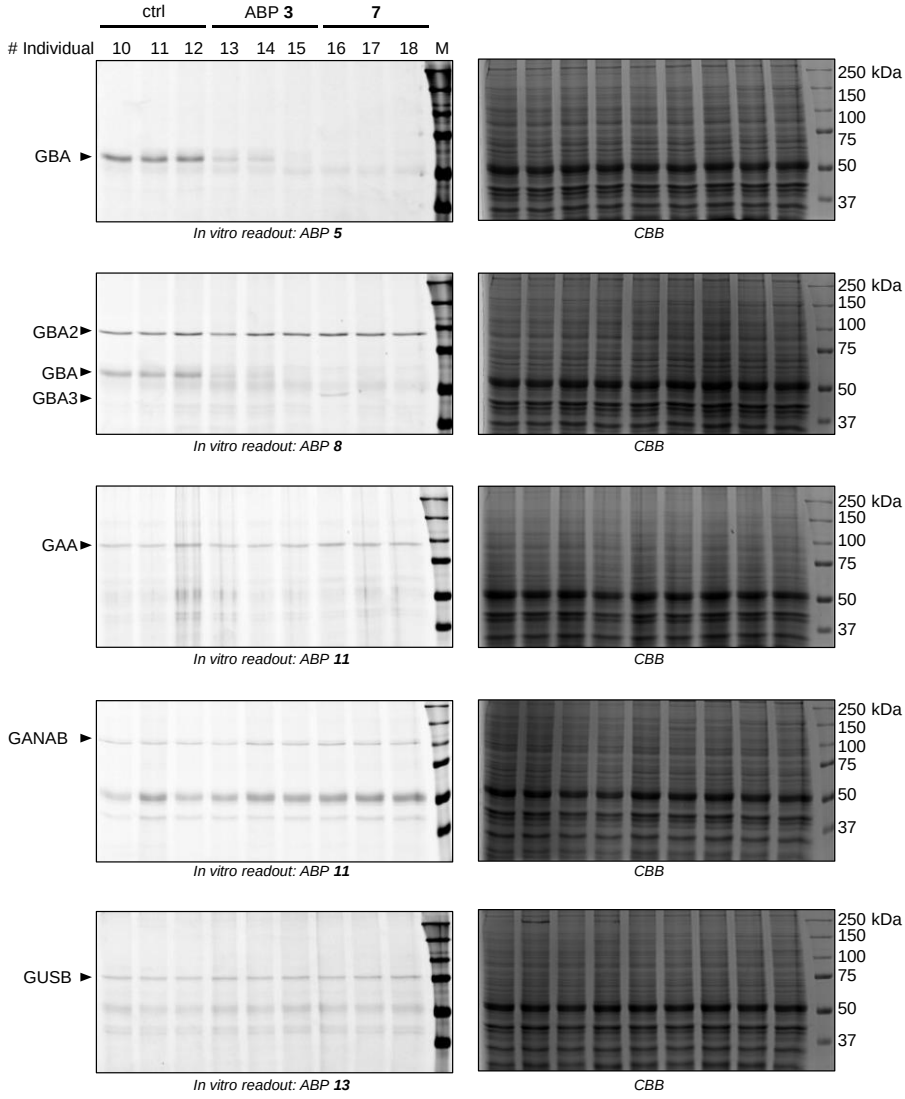

Figure 3.S7 (continued, 2 of 4).

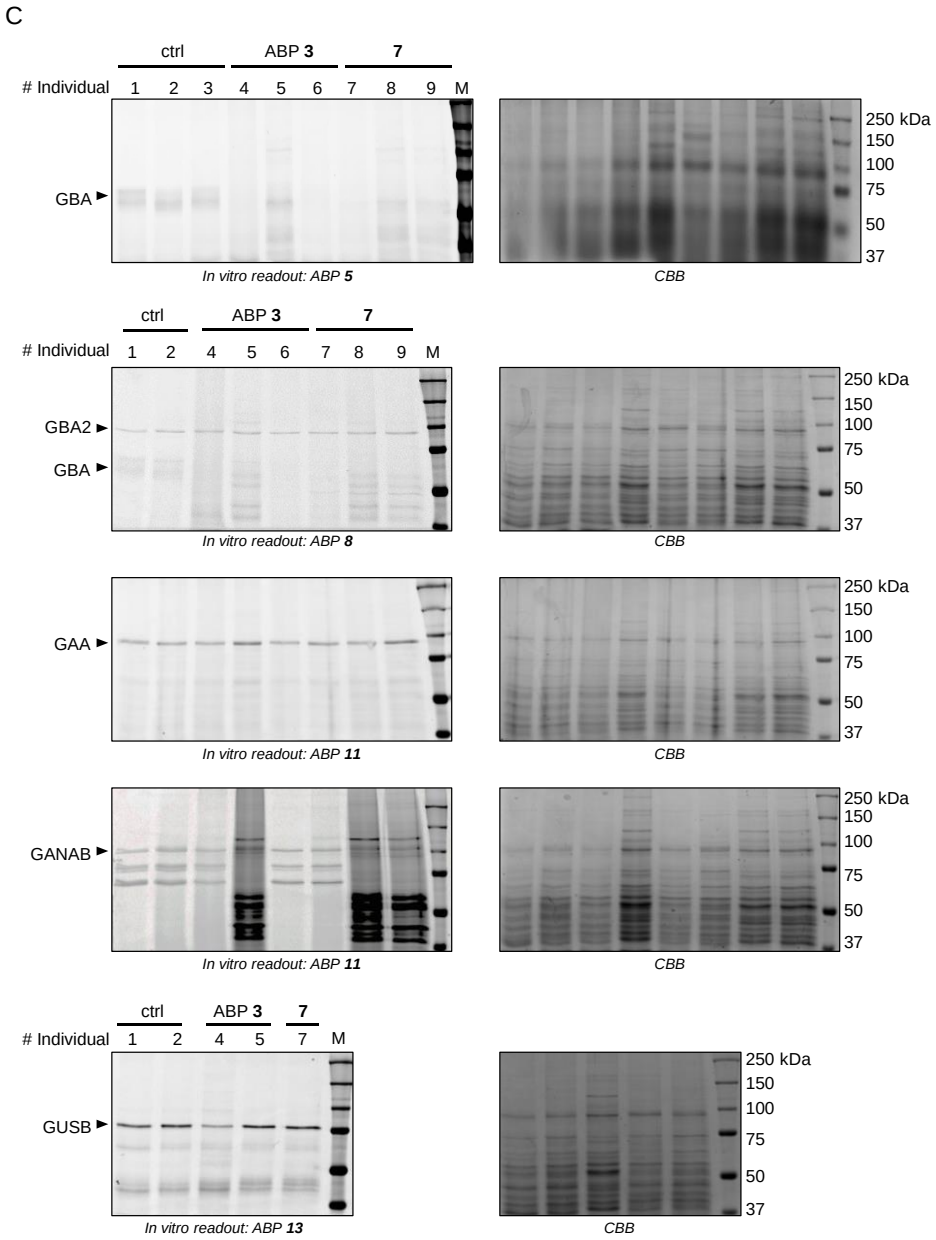

Figure 3.S7 (continued, 3 of 4).

D

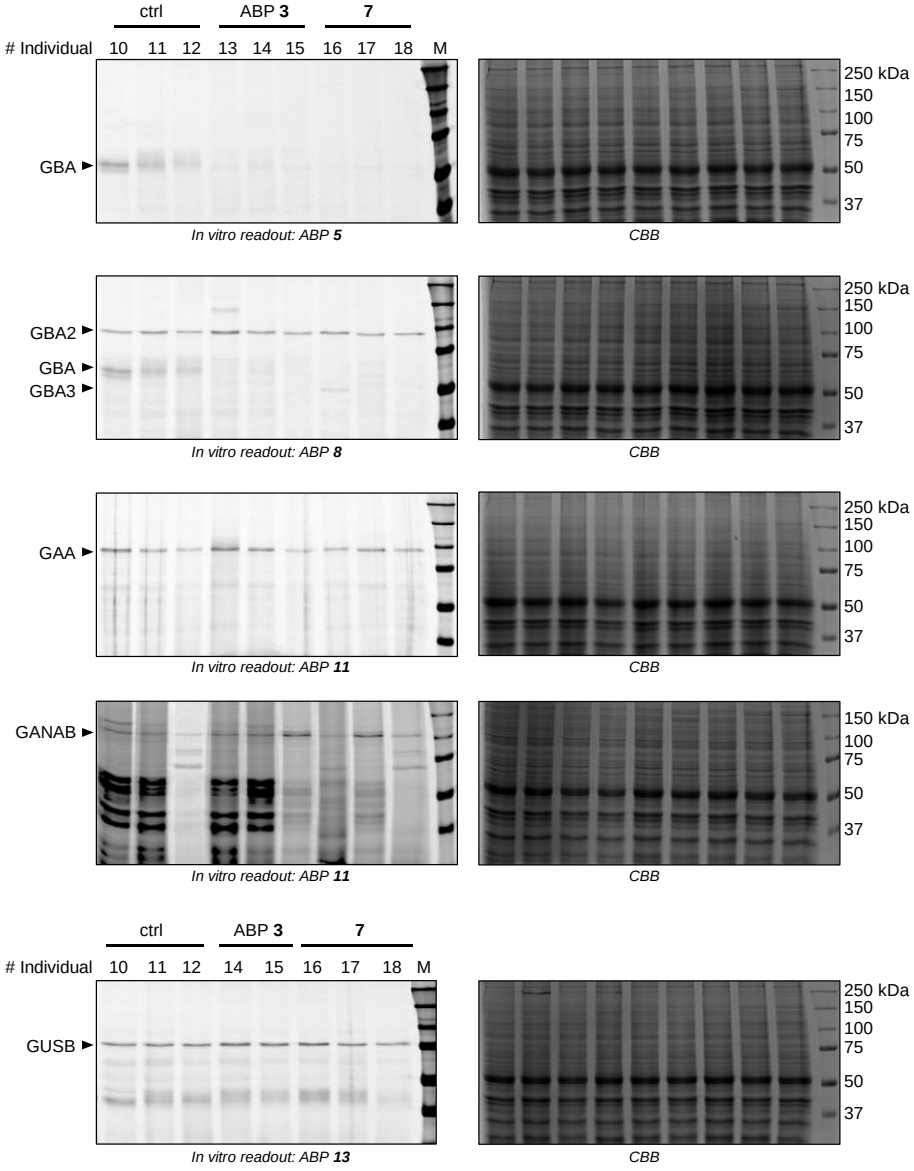

Figure 3.S7. *In vivo* targets of ABPs 3 and inhibitor 7 of treated adult zebrafish revealed by competitive ABPP. A), B) labeling in brain homogenates C), D) Labeling in liver and spleen homogenates. *CBB*, Coomassie brilliant blue stain.

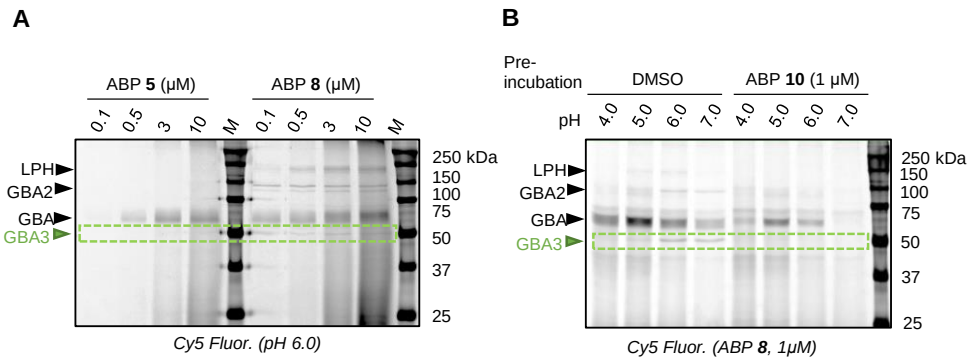

Figure 3.S8. Detection of GBA3 in lysates of zebrafish larvae. A) Labeling using ABP **5** (ME569) or ABP **8** (JJB367) at various ABP concentrations. B) Labeling using ABP **8** (JJB367) in lysates at various pH, with or without pre-incubation of ABP **10** (JJB70).

Table 3.S1. Data collection and refinement statistics for rGBA in complex with ABP **5** and inhibitors **6** and **7**.

	5	**6**	**7**
Data collection			
Space group	*C* 2 2 2_1	*C* 2 2 2_1	*C* 2 2 2_1
Cell dimensions			
a, *b*, *c* (Å)	110.6, 285.9, 92.3	110.4, 285.2, 91.9	110.2, 285.1, 92.0
α, β, γ (°)	90, 90, 90	90, 90, 90	90, 90, 90
Resolution (Å)	77.52-1.92 (1.95-1.92)*	72.13-1.63 (1.66-1.63)	71.98-1.81 (1.84-1.81)
R_{merge}	0.161 (1.623)	0.101 (1.609)	0.132 (1.661)
R_{pim}	0.064 (0.647)	0.047 (0.735)	0.061 (0.757)
I / σI	6.5 (1.1)	8.8 (1.1)	7.7 (1.0)
Completeness (%)	99.9 (99.8)	99.9 (98..8)	100.0 (98.7)
Redundancy	8.3 (8.1)	6.49 (6.50)	6.53 (6.58)
Refinement			
Resolution (Å)	77.52-1.92	72.13-1.63	71.98-1.81
No. reflections	925691	1167262	859243
R_{work} / R_{free}	0.18/0.22	0.18/0.21	0.18/0.21
No. atoms			
Protein	7939	7870	7960
Ligand/ion	354	273	334
Water	699	966	936
B-factors (Å^2)			
Protein	39	26	28
Ligand/ion	65	52	55
Water	47	39	39
R.m.s. deviations			
Bond lengths (Å)	0.009	0.012	0.010
Bond angles (°)	1.60	1.67	1.63
Ramachandran Plot Residues			
In most favourable regions (%)	94.5	94.7	94.6
In allowed regions (%)	4.3	4.2	4.3
PDB code	6Q6K	6Q6N	6Q6L

*Values in parentheses are for highest-resolution shell.

Table 3.S2. Lipophilic ligand efficiency (LipE) values of CBE **1**, CP **2**, ABP **3**, ABP **5** and new functionalized cyclophellitol **6** and **7** for rGBA activity. LipE = pIC_{50} – cLogP. cLogP values were calculated using the ChemDraw version 16 software.

	CBE 1	**CP** 2	**ABP** 3	**ABP** 5	6	7
cLogP	-1.76	-2.77	2.47	1.66	1.16	1.60
pIC_{50} GBA	5.37	7.52	9.00	8.52	9.00	9.00
LipE	7.13	10.29	6.53	6.86	7.84	7.40

3.S1 Crystallographic data collection and refinement statistics (University of York)

3.S1.1 Deglycosylation, Purification and Crystallization

Prior to crystallization, Cerezyme (3.4 mg mL^{-1}, NEB) was deglycosylated with PNGase F (20 μL, NEB) for 5 days at room temperature. The digested material was purified by size exclusion chromatography on an S75 16/600 column. Crystals were obtained using hanging-drop vapor diffusion, based on parent conditions outlined by Dvir et al. (2003).[1] Drops contained 1 μL purified Cerezyme (9.1 mg mL^{-1}) and 1 μL mother liquor (1.1 M $(NH_2)_2SO_4$, 0.19 M guanidine HCl, 0.04 M KCl, 0.1 M Na acetate, pH 4.6). Crystals were grown for 1 week at 18 °C.

3.S1.2 Inhibitor Complexes

Inhibitors were prepared at 20 mM in HEPES buffer (20 mM, pH 7.0) and diluted to 2 mM in mother liquor comprising 1.1 M $(NH_2)_2SO_4$, 0.19 M guanidine HCl, 0.04 M KCl and 0.1 M Na acetate (pH 4.6). Crystals were soaked in 5 μL of inhibitor-mother liquor solution for 4 hours at 18 °C. Crystals were transferred to a lithium sulfate cryoprotectant (0.2 M Li_2SO_4, 0.17 M guanidine HCl, 0.04 M KCl, 0.1 M Na acetate, pH 4.6) before freezing in liquid nitrogen.

3.S1.3 Structure Solution and Refinement

For the ABP **5** complex, data were collected at the i04_1 beamline of the Diamond Light Source Facility to 1.79 Å. Data were collected at the i24 beamline to 1.81 Å and 1.63 Å for the inhibitors **6** and **7** complexes respectively. For all complexes, data were processed using the XIA2[2, 3] and AIMLESS data reduction pipelines through the CCP4i2 software.[4] The structures were solved by molecular replacement using MOLREP[5] with the previous GBA1 PDB (2NT0)[6] as the homologous search model. Refinement was performed using REFMAC[7] followed by several rounds of manual model building with COOT.[8] Idealised coordinate sets and refinement dictionaries for the ligands were generated using JLIGAND[9] and sugar conformations were validated using Privateer.[10] Crystal structure figures were generated using ccp4mg.[11] For ABP **5**, the structure could be traced from residues 1–497 in chain A and chain B. In chain A, residue 344 is disordered in density and has been omitted. In chain B residues 29–31 and 346–348 are disordered in density and have been omitted. For inhibitor **6**, the structure could be traced from residues 1–497 in chain A and chain B. In chain B, residues 344–345 are disordered in density and have been omitted.

For inhibitor **7** the structure could be traced from residues 1–497 in chain A and chain B. In chain A, residue 345 is disordered in density and has been omitted. In chain B, residues 316–318 and residues 344–347 are disordered in density and have been omitted.

3.S2 Synthesis of ABP 5 and Compounds 6 and 7 (Department of Bio-organic Synthesis, Leiden University)

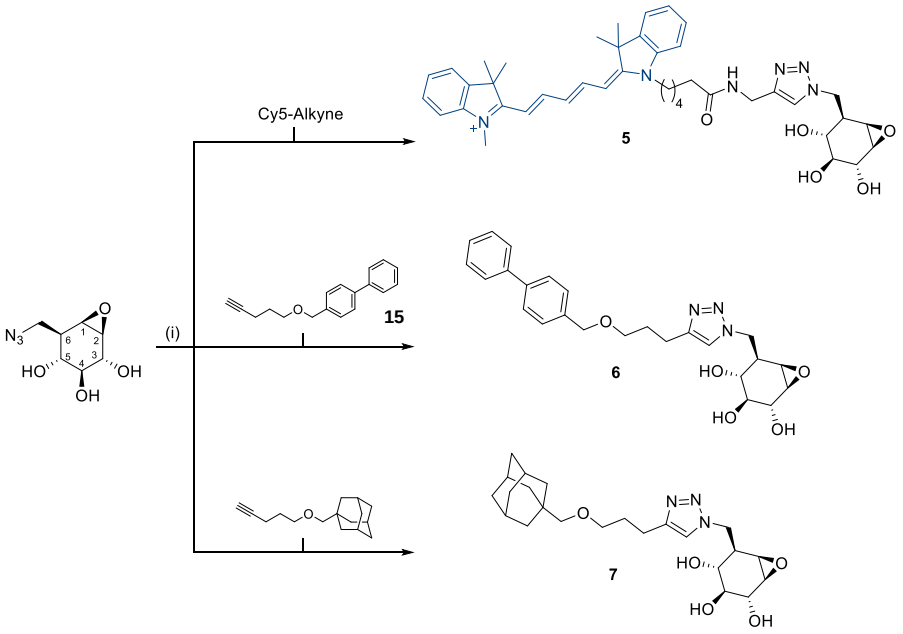

Scheme 3.S1. Synthesis of C-8 functionalized cyclophellitol ABP 5 and inhibitors 6 and 7. Reagents and conditions: (i) $CuSO_4 \cdot H_2O$, sodium ascorbate, DMF, RT, 18 h, **5**: 38%, **6**: 78%, **7**: 89%.

3.S2.1 4-((pent-4-yn-1-yloxy)methyl)-1,1'-biphenyl (**15**)

[1,1'-biphenyl]-4-ylmethanol (689 mg, 3.74 mmol), tetrabutyl ammonium iodide (1.38 g, 3.74 mmol) and NaH (204 mg, 5.10 mmol) were added to a cooled (0 °C) solution of 5-bromopent-1-yne (500 mg, 3.74 mmol) in DMF (15 mL). The reaction mixture was allowed to warm to room temperature and stirred 24 h and subsequently poured into ice, extracted with EtOAc (20 mL), and washed with water (20 mL) and saturated aqueous NaCl (10 mL). The organic phase was dried ($MgSO_4$), filtered and concentrated. The residue was purified by silica gel column chromatography with Pentane/EtOAc (from 10:0 to 8:2, v/v) to give the desired product as a yellow oil (102 mg, mmol, 12% yield). ^{1}H-NMR (300 MHz, $CDCl_3$) δ 7.62 – 7.49 (m, 4H, 4 x

CH Ar), 7.49 – 7.28 (m, 5H, 5 x CH Ar), 4.54 (s, 2H, CH_2O), 3.59 (t, J = 6.1 Hz, 2H, CH_2O), 2.33 (td, J = 7.1, 2.7 Hz, 2H, CH_2), 1.94 (t, J = 2.7 Hz, 1H, CH), 1.91 – 1.78 (m, 2H, CH_2); ^{13}C-NMR (101 MHz, $CDCl_3$) δ 141.0, 140.6, 137.6, 128.9, 128.7, 128.4, 128.2, 127.4, 127.3, 127.2, 84.1, 72.8, 68.8, 68.6, 28.8, 15.4. LC/MS: (linear gradient 10%→90% B in 12.5 min), m/z 251.1 $[M+H]^+$.

3.S2.2 (1*S*,2*R*,3*S*,4*R*,5*R*,6*R*)-5-((4-(3-([1,1'-biphenyl]-4-ylmethoxy)propyl)-1H-1,2,3-triazol-1-yl)methyl)-7-oxabicyclo[4.1.0]heptane-2,3,4-triol (**6**)

Azido cyclophellitol[12] (4.4 mg, 0.022 mmol) was dissolved in DMF (1 mL) and $CuSO_4 \cdot 5H_2O$ (0.1 M, 50 µL, 4.4 µmol, 0.2 eq.) and sodium ascorbate (0.1 M, 50 µL, 4.4 µmol, 0.2 eq.) were added to the solution under argon atmosphere. Then, a solution of biphenyl alkyne (4.4 mg, 26 µmol, 1.2 eq.) was added and the reaction mixture was stirred at room temperature for 18 h. The crude was purified by column chromatography (DCM to DCM/MeOH 9:1) to afford the desired compound **6** (7.7 mg, 0.017 mmol, 78%). Rf: 0.20 (DCM/MeOH 9:1). ^{1}H-NMR (400 MHz, CD_3OD) δ 7.65 – 7.55 (m, 4H, 4 x CH Ar), 7.43 (t, J = 7.7 Hz, 4H, 4 x CH Ar), 7.32 (t, J = 7.4 Hz, 1H, CH Ar), 5.49 (s, 1H, CH=N), 4.81 (d, J = 14.3 Hz, 1H, C*H*H-7), 4.69 – 4.56 (m, 1H, CH*H*-7), 4.55 (s, 2H, CH_2O), 3.65 – 3.48 (m, 3H, CH_2O, CH-2), 3.21 (t, J = 8.8 Hz, 1H, CH-3), 3.17 – 3.06 (m, 1H, CH-4), 3.02 – 2.97 (s, 2H, CH-1, CH-6), 2.85 (br s, 2H, CH_2), 2.40 – 2.35 (t, J = 7.3 Hz, 1H, CH-5), 2.03 (br s, 2H, CH_2); ^{13}C-NMR (101 MHz, CD_3OD) δ 142.1, 141.8, 138.93 (3 x C Ar), 131.1, 129.9, 129.4, 128.4, 127.9 (9 x CH Ar), 78.2 (CH-4), 73.6 (CH_2O), 72.5 (CH-2), 70.1 (CH_2O), 68.7 (CH-3), 57.5, 55.5 (CH-1/CH-6), 51.1 (CH_2), 44.5 (CH-5), 30.2 (CH_2). HRMS: calculated for $C_{25}H_{30}N_3O_5^+$ $[M+H]^+$ 452.21855, found: 452.21759.

3.S2.3 (1*S*,2*R*,3*S*,4*R*,5*R*,6*R*)-5-((4-(3-(((1*s*,3*S*)-adamantan-1-yl)methoxy)propyl)-1*H*-1,2,3-triazol-1-yl)methyl)-7-oxabicyclo[4.1.0]heptane-2,3,4-triol (**7**)

Azido-cyclophellitol[12] (4.4 mg, 0.022 mmol) was dissolved in DMF (1 mL) and $CuSO_4 \cdot 5H_2O$ (0.1 M, 50 µL, 4.4 µmol, 0.2 eq.) and sodium ascorbate (0.1 M, 50 µL, 4.4 µmol, 0.2 eq.) were added to the solution under argon atmosphere. Then, a solution of adamantane alkyne (6.10 mg, 26 µmol, 1.2 eq.) was added and the reaction mixture was stirred at room temperature for 18 h. The crude was purified by column chromatography (DCM to DCM/MeOH 9:1) to afford the desired compound **7** (8.4 mg, 0.019 mmol, 89%). Rf: 0.20 (DCM/MeOH 9:1). ^{1}H-NMR (400 MHz, CD_3OD) δ 4.82 (dd, J = 13.7, 3.9 Hz, 1H, CH*H*), 4.62 (dd, J = 13.8, 8.5 Hz, 1H, C*H*H),

3.62 (d, *J* = 8.1 Hz, 1H, CH-2), 3.42 (t, *J* = 5.4 Hz, 2H, CH_2), 3.23 (dd, *J* = 10.0, 8.1 Hz, 1H, CH-3), 3.13 (t, *J* = 9.8 Hz, 1H, CH-4), 3.03 (s, 2H, CH-1, CH-6), 2.97 (s, 2H, CH_2O), 2.80 (br s, 2H, CH_2), 2.39 (td, *J* = 9.0, 3.5 Hz, 1H, CH-5), 1.95 (br s, 4CH, 4 x CH adamantane), 1.85 – 1.63 (m, 6H, 3 x CH_2 adamantane), 1.57 (br s, 6H, 3 x CH_2 adamantane); ^{13}C-NMR (101 MHz, CD_3OD) *δ* 83.0 (CH_2O), 78.2 (CH-3), 72.5 (CH-2), 71.4 (CH_2), 68.7 (CH-4), 57.6, 55.5 (CH-1/CH-6), 44.6 (CH-5), 40.8 (3 x CH_2), 38.3 (3 x CH_2), 35.1 (C adamantane), 30.3 (CH_2), 29.8 (4 x CH adamantane), 23.2 (CH_2); HRMS: calculated for $C_{25}H_{30}N_3O_5^+$ $[M+H]^+$ 434.26550, found: 434.26441.

3.S2.4 Cyclophellitol Cy5 ABP (**5**)

Azido-cyclophellitol[12] (24.2 mg, 0.12 mmol) and the desired Cy5-alkyne (84 mg, 0.15 mmol) were dissolved in BuOH/toluene/H_2O (6 mL, 1:1:1, v/v/v). $CuSO_4$ (0.024 mL, 1 M in H_2O) and sodium ascorbate (0.024 mL, 1 M in H_2O) were added and the reaction mixture was heated at 80 ºC for 18 h. Then, the solution was diluted with CH_2Cl_2, washed with H_2O, dried over $MgSO_4$ and concentrated under reduced pressure. The crude was purified by silica gel column chromatography (CH_2Cl_2 to CH_2Cl_2/MeOH 9:1), subsequently purified by semipreparative reversed-phase HPLC (linear gradient: 45 to 48% B in A, 12 min, solutions used A: 50mM NH_4HCO_3 in H_2O, B: MeCN) and lyophilized to yield ABP **5** as a blue powder (33.5 mg, 44 μmol, 37%). ^{1}H NMR (400 MHz, CD_3OD): *δ* 8.25 (t, *J* = 13.1 Hz, 2H), 7.91 (d, *J* = 3.3 Hz, 1H), 7.49 (d, *J* = 7.4 Hz, 2H), 7.44 – 7.39 (m, 2H), 7.31 – 7.24 (m, 4H), 6.63 (t, *J* = 12.4 Hz, 1H), 6.29 (d, *J* = 13.8 Hz, 2H), 4.81 (dd, *J* = 13.9, 3.8 Hz, 1H), 4.61 (dd, *J* = 13.9, 8.6 Hz, 1H), 4.42 (s, 2H), 4.09 (t, *J* = 7.4 Hz, 2H), 3.63 (s, 3H), 3.60 (d, *J* = 8.0 Hz, 1H), 3.24 – 3.20 (m, 1H), 3.12 (t, *J* = 14.9 Hz, 1H), 3.02 – 3.00 (m, 1H), 2.41 – 2.35 (m, 1H), 2.25 (t, *J* = 7.3 Hz, 2H), 1.91 (s, 6H), 1.85 – 1.78 (m, 2H), 1.72 (s, 12H), 1.50 – 1.43 (m, 2H) ppm; ^{13}C NMR (101 MHz, CD_3OD): *δ* 175.8, 175.4, 174.6, 155.5, 155.5, 146.2, 144.2, 143.5, 142.6, 142.5, 129.8, 129.7, 126.7, 126.2, 126.2, 125.2, 123.4, 123.3, 112.0, 111.8, 104.5, 104.3, 78.2, 72.5, 68.6, 57.6, 55.5, 50.8, 50.5, 50.5, 44.8, 44.6, 36.5, 35.6, 31.6, 28.1, 28.0, 27.3, 26.4 ppm; HRMS: calculated for $C_{42}H_{53}N_6O_5$ $[M]^+$ 721,4072, found: 721.4070.

3.S3 Supplementary References

1 Dvir H, Harel M, McCarthy AA, Toker L, Silman I, Futerman AH & Sussman JL (2003) X-Ray Structure of Human Acid-β-Glucosidase, the Defective Enzyme in Gaucher Disease. *EMBO Rep* **4**, 704–709.

2 Kabsch W (2010) XDS. *Acta Crystallogr. D. Biol. Crystallogr.* **66**, 125–132.

3 Winter G. (2010) Xia2: An Expert System for Macromolecular Crystallography Data Reduction. *J. Appl. Crystallogr.* **43**, 186–190.

4 Winn MD, Ballard CC, Cowtan KD, Dodson EJ, Emsley P, Evans PR, Keegan RM, Krissinel EB, Leslie AG, McCoy A, McNicholas SJ, Murshudov GN, Pannu NS, Potterton EA, Powell HR, Read RJ, Vagin A & Wilson KS (2011) Overview of the CCP4 Suite and Current Developments. *Acta Crystallogr Sect D Biol Crystallogr* **67**, 235–242.

5 Vagin A, Teplyakov A (2010) Molecular Replacement with MOLREP. *Acta Crystallogr Sect D Biol Crystallogr* **66**, 22–25.

6 Lieberman RL, Wustman BA, Huertas P, Powe A C, Pine CW, Khanna R, Schlossmacher MG, Ringe D & Petsko GA (2007) Structure of Acid β-Glucosidase with Pharmacological Chaperone Provides Insight into Gaucher Disease. *Nat Chem Biol* **3**, 101–107.

7 Murshudov GN, Vagin, AA & Dodson EJ (1997) Refinement of Macromolecular Structures by the Maximum-Likelihood Method. *Acta Crystallogr Sect D Biol Crystallogr* **53**, 240–255.

8 Emsley P & Cowtan K (2004) Coot: Model-Building Tools for Molecular Graphics. *Acta Crystallogr Sect D Biol Crystallogr* **60**, 2126–2132.

9 Lebedev AA, Young P, Isupov MN, Moroz OV, Vagin AA, & Murshudov GN (2012) JLigand: A Graphical Tool for the CCP4 Template-Restraint Library. *Acta Crystallogr Sect D Biol Crystallogr* **68**, 431–440.

10 Agirre J, Iglesias-Fernández J, Rovira C, Davies GJ, Wilson KS & Cowtan KD (2015) Privateer: Software for the Conformational Validation of Carbohydrate Structures. *Nat Struct Mol Biol* **22**, 833–834.

11 McNicholas S, Potterton E, Wilson KS & Noble MEM (2011) Presenting Your Structures: The CCP4mg Molecular-Graphics Software. *Acta Crystallogr Sect D Biol Crystallogr* **67**, 386–394.

12 Li KY, Jiang J, Witte MD, Kallemeijn WW, Van Den Elst H, Wong CS, Chander SD, Hoogendoorn S, Beenakker TJM, Codée JDC, Aerts JM, van der Marel GA & Overkleeft HS (2014) Synthesis of Cyclophellitol, Cyclophellitol Aziridine, and Their Tagged Derivatives. *European J Org Chem* **2014**, 6030–6043.